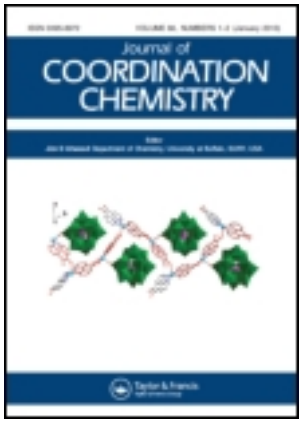

Journal of Coordination Chemistry
Publication details, including instructions for authors and subscription information:
http://www.tandfonline.com/loi/gcoo20

Synthesis, characterization, DNA interaction, cytotoxicity, and apoptosis induction of a mixed-ligand copper(II) complex

Cheng-Zhi Xie[a], Meng-Meng Sun[a], Shao-Hua Li[a], Xiao-Tong Zhang[a], Xin Qiao[a], Yan Ouyang[a] & Jing-Yuan Xu[a]

[a] Tianjin Key Laboratory on Technologies Enabling Development of Clinical Therapeutics and Diagnostics, School of Pharmacy, Tianjin Medical University, Tianjin, P.R. China

Accepted author version posted online: 18 Oct 2013.Published online: 26 Nov 2013.

To cite this article: Cheng-Zhi Xie, Meng-Meng Sun, Shao-Hua Li, Xiao-Tong Zhang, Xin Qiao, Yan Ouyang & Jing-Yuan Xu (2013) Synthesis, characterization, DNA interaction, cytotoxicity, and apoptosis induction of a mixed-ligand copper(II) complex, Journal of Coordination Chemistry, 66:22, 3891-3905, DOI: 10.1080/00958972.2013.857015

To link to this article: http://dx.doi.org/10.1080/00958972.2013.857015

Journal of Coordination Chemistry, 2013
Vol. 66, No. 22, 3891–3905, http://dx.doi.org/10.1080/00958972.2013.857015

Synthesis, characterization, DNA interaction, cytotoxicity, and apoptosis induction of a mixed-ligand copper(II) complex

CHENG-ZHI XIE, MENG-MENG SUN, SHAO-HUA LI, XIAO-TONG ZHANG, XIN QIAO, YAN OUYANG and JING-YUAN XU*

Tianjin Key Laboratory on Technologies Enabling Development of Clinical Therapeutics and Diagnostics, School of Pharmacy, Tianjin Medical University, Tianjin, P.R. China

(*Received 27 June 2013; accepted 18 September 2013*)

A mixed-ligand complex, $[Cu(Hptc)(Me_2bpy)(H_2O)]\cdot 3H_2O$ (**1**) (H_3ptc = pyridine-2,4,6-tricarboxylic acid; Me_2bpy = 4,4′-dimethyl-2,2′-dipyridine), has been synthesized and characterized by elemental analysis, IR, and single-crystal X-ray diffraction. In the discrete mononuclear structure of **1**, the copper core is in a distorted octahedral environment (CuN_3O_3) derived from tridentate chelate $Hptc^{2-}$, bidentate chelate Me_2bpy and a coordinated water. The interaction of **1** with CT-DNA was investigated by UV–vis spectra, fluorescence spectra and viscosity, which reveals that **1** binds to CT-DNA by partial intercalation. Gel electrophoresis assay demonstrated that the complex displays efficient oxidative cleavage of supercoiled DNA with H_2O_2 as an oxidant. The *in vitro* cytotoxicity of **1** on HeLa cells was assessed by MTT and clonogenic assay, where IC_{50} equals 4.24 ± 0.03 μM. Fluorescence microscopic observations indicated that **1** can induce apoptosis of HeLa cells.

Keywords: Copper complex; Pyridine-2,4,6-tricarboxylic acid; DNA interaction; Cytotoxicity; Apoptosis

1. Introduction

Inorganic medicinal chemistry is a multidisciplinary field combining elements of chemistry, pharmacology, toxicology, and biochemistry, which turn out to be particularly of growing significance in both therapeutic and diagnostic medicine [1–4]. The clinical success of cisplatin, carboplatin, oxaliplatin, and other platinum-based antitumor complexes have promoted the development of metal-based drugs. However, all these platinum-based drugs are associated with high toxicity, serious side effects and evolution of drug resistance during therapy. To overcome these problems, there is an urgent medical need for seeking and developing more effective, less toxic, and target-specific metal-based anticancer drugs [5]. Synthesis, DNA-binding and cytotoxic activity of platinum(II) complexes with substituted pyridine derivatives have been well documented. Among these, platinum(II) complexes containing pyridine carboxylic acids have received great attention as potential anticancer metal complexes. In some cases, the activity of these complexes was comparable with that of cisplatin [6–8].

*Corresponding author. Email: xujingyuan@tmu.edu.cn
Cheng-Zhi Xie and Meng-Meng Sun contributed equally to this work.

It is generally accepted that DNA is the primary biological target of the metal-based anticancer drug, although there is some evidence to suggest that other biological targets may be important in the mechanism [9]. Apoptosis, known as programmed cell death, is a crucial process related to a number of diseases, especially cancer. Drug-induced activation of specific signaling pathways is always concerned with controlled cell apoptosis [10, 11]. Designing and synthesizing novel complexes capable of interacting with DNA and triggering apoptosis is currently one of the most promising strategies for researchers to discover novel DNA-targeted anticancer drugs for chemotherapy [12–15]. In addition, if a complex exhibits IC_{50} values that are close to or less than cisplatin for the same cell line, it is a potentially promising drug for cancer.

It is known that copper is a bio-essential element with relevant oxidation states. Cu(II) complexes are capable of interacting with nuclear proteins and DNA, causing site-specific damage, increasing cell death and causing apoptosis in different cell cultures, which have garnered increasing attention of inorganic chemists [16–19]. Since Dwyer reported the inhibition of landschütz ascites tumor growth by $[Cu(tmphen)_2]Cl_2$ (where tmphen stands for 3,4,7,8-tetramethyl-1,10-phenanthroline) [20], anticancer properties of a wide range of copper complexes containing nitrogen-containing heterocyclic ligands have been intensively investigated [17, 19, 21–25]. Cu(II) mixed-ligand antineoplastic agents, containing 1,10-phenanthroline (phen) or 2,2′-bipyridine (bpy) derivatives in combination with carboxylic acid ligands, have been reported, which exhibit cytotoxicity, genotoxicity, and antitumor effects [26–28]. However, the mechanism by which these complexes enforce their biological activity is still unknown. In order to widen the scope of investigations on new biologically active pharmaceuticals, we are trying to synthesize new mixed-ligand copper (II) complexes and study their DNA interactions and anticancer properties. In our study, except the chelating Me_2bpy ligand (4,4′-dimethyl-2,2′-dipyridine), we have also chosen as co-ligand H_3ptc (pyridine-2,4,6-tricarboxylic acid) because the multifunctional ligand H_3ptc bearing three carboxyl groups and one N atom which are potential donors acting as metal acceptors is extremely adequate. Herein, we present the synthesis, structure, DNA binding, DNA cleavage activity, cytotoxicity, and apoptosis induction of a new mixed-ligand copper (II) complex.

2. Experimental

2.1. *Materials and instrumentation*

All chemicals and reagents were purchased from commercial sources and used without purification. H_3ptc was synthesized according to a previously reported procedure [29]. Ethidium bromide (EB), 3-(4,5-dimethylthiazol-2-yl)-2,5-diphenyltetrazolium bromide (MTT), crystal violet, Hoechst 33342, calf thymus DNA (CT-DNA), supercoiled plasmid pUC19 DNA, and high glucose DMEM were purchased from Sigma. The tris(hydroxymethyl)aminomethane (Tris-) HCl buffer solution was prepared with triply-distilled water. Fetal bovine serum (FBS) was obtained from Hyclone. CT-DNA stock solution was prepared by diluting DNA with Tris–HCl/NaCl buffer (pH = 7.2, 5 mM Tris–HCl, 50 mM NaCl) and kept at 4 °C for no longer than a week. The UV absorbance at 260 and 280 nm of CT-DNA solution in Tris buffer gave a ratio of 1.8–1.9, indicating that the DNA was sufficiently free of protein [30]. The concentration of CT-DNA was determined from its absorption intensity at 260 nm with a molar extinction coefficient of 6600 M^{-1} cm^{-1} [31].

Elemental analyzes for C, H, and N were obtained on a Perkin-Elmer analyzer model 240. Infrared spectroscopy on KBr pellets was performed on a Bruker Vector 22 FT-IR spectrophotometer from 4000–400 cm^{-1}. The electronic spectra were measured on a JASCO V-570 spectrophotometer. The fluorescence spectral data were obtained on a MPF-4 fluorescence spectrophotometer at room temperature. The Gel Imaging and Documentation Digi Doc-It System were assessed by Labworks Imaging and Analysis Software (UVI, UK).

2.2. *Synthesis of [Cu(Hptc)(Me$_2$bpy)(H$_2$O)]·3H$_2$O (1)*

A deionized aqueous solution (12 mL) containing $Cu(NO_3)_2 \cdot 6H_2O$ (0.3 mM, 64.2 mg), H_3ptc (0.3 mM, 63.5 mg) and Me_2bpy (0.3 mM, 54.9 mg) was stirred and refluxed for 6 h. The mixture was then cooled to room temperature and filtered. The filtrate was allowed to stand at room temperature for 6 days and resulted in the formation of blue rhombus crystals. Yield: 31%. Anal. Calcd for $C_{20}H_{23}Cu\ N_3O_{10}$ (%): C, 45.41; H, 4.38; N, 7.94. Found: C, 45.69; H, 4.27; N, 7.87. IR spectrum (KBr pellet, cm^{-1}): 3424m, 3060m, 1618vs, 1559m, 1416m, 1346s, 1291m, 1255s, 1032m, 922m, 840m, 773m, 733m, 693m.

2.3. *X-ray crystallography*

Room temperature (294 ± 1 K) single-crystal X-ray experiments were performed on a Bruker SMART 1000 CCD diffractometer equipped with graphite monochromated MoKα radiation. Data collection and reduction were performed using SMART and SAINT software [32]. An empirical absorption correction (SADABS) was applied to the raw intensities [33]. The structure was solved by direct methods and refined by full-matrix least squares based on F^2 using the SHELXTL program package. Nonhydrogen atoms were subjected to anisotropic refinement [34]. Hydrogens were assigned with common isotropic displacement factors. Hydrogens were included at geometrically calculated positions and refined using a riding model except for those bonded to the oxygens in water, which were located on a difference Fourier map. Crystallographic data for **1** is listed in table 1. Selected bond lengths and angles are listed in table 2.

2.4. *DNA-binding and cleavage experiments*

Absorption titration experiments were carried out in Tris–HCl/NaCl buffer at room temperature to investigate the binding affinity between CT-DNA and **1**. About 2 mL blank Tris–HCl/NaCl buffer solution and buffered Cu(II) complex solution ([complex] = 2×10^{-5} M) were placed into two 1 cm path cuvettes, respectively, and then, gradually, the concentration of DNA (25–200 μM) was increased. While measuring the absorption spectra, an aliquot (5 μL) of buffered CT-DNA solution (0.01 M) was added step by step to each cuvette to eliminate the absorbance of DNA itself.

The relative binding of **1** to CT-DNA was determined with an EB-bound CT-DNA solution in Tris–HCl/NaCl buffer (pH = 7.2, 5 mM Tris–HCl, 50 mM NaCl). The experiments were carried out by adding a certain amount of solution of **1** step by step into the EB-DNA solution (4.0×10^{-6} M EB and 80×10^{-6} M CT-DNA). The influence of the addition of **1** to the EB-DNA complex was obtained by recording the variation of fluorescence emission spectra with excitation at 510 nm and emission at 606 nm.

Table 1. Crystal data and structure refinement information for **1**.

Empirical formula	$C_{20}H_{23}CuN_3O_{10}$
Formula weight	528.96
Temperature (K)	294(1)
Wavelength (Å)	0.71073
Crystal system	Monoclinic
Space group	$P_2(1)/c$
a (Å)	9.2680(19)
b (Å)	11.401(2)
c (Å)	21.000(4)
β (°)	91.86(3)
Volume (Å^3), Z	2217.8(7), 4
Calculated density (kg/m^3)	1.584
Absorption coefficient (mm^{-1})	1.048
F(000)	1092
θ Range for data collection (°)	3.02–27.51
Independent reflections	5033
Observed reflections	15,667
Refinement method	Full-matrix least-squares on F^2
Data/restraints/parameters	5033/0/343
Goodness-of-fit on F^2	1.064
Final R indices [$I > 2\sigma(I)$]	$R_1 = 0.0613$, w$R_2 = 0.1277$
R indices (all data)	$R_1 = 0.0913$, w$R_2 = 0.1398$
Largest diff. peak and hole	0.766 and −1.028 Å^{-3}

Table 2. Selected bond lengths (Å) and angles (°) for **1**.

Cu(1)–N(3)	1.972(3)	Cu(1)–O(7)	1.988(3)
Cu(1)–N(1)	2.011(3)	Cu(1)–N(2)	2.018(3)
Cu(1)–O(6)	2.258(3)	Cu(1)–O(4)	2.323(2)
O(1)–C(13)	1.304(4)	O(2)–C(13)	1.200(4)
O(3)–C(5)	1.249(4)	O(4)–C(5)	1.238(4)
O(5)–C(11)	1.235(4)	O(6)–C(11)	1.242(4)
N(3)–Cu(1)–O(7)	91.33(12)	N(3)–Cu(1)–N(1)	176.79(10)
O(7)–Cu(1)–N(1)	91.20(11)	N(3)–Cu(1)–N(2)	80.67(11)
O(7)–Cu(1)–N(2)	170.03(13)	N(1)–Cu(1)–N(2)	97.01(11)
N(3)–Cu(1)–O(6)	102.25(10)	O(7)–Cu(1)–O(6)	90.78(12)
N(1)–Cu(1)–O(6)	75.73(10)	N(2)–Cu(1)–O(6)	96.70(10)
N(3)–Cu(1)–O(4)	107.13(10)	O(7)–Cu(1)–O(4)	86.99(11)
N(1)–Cu(1)–O(4)	74.98(9)	N(2)–Cu(1)–O(4)	89.69(10)
O(6)–Cu(1)–O(4)	150.57(9)		

Viscosity measurement of 100 μM CT-DNA in Tris–HCl/NaCl buffer was performed using an Ubbelodhe viscometer with the temperature setting at 30 ± 0.1 °C in a constant temperature bath. Data are presented as $(\eta/\eta_0)^{1/3}$ *versus* binding ratio [Complex]/[DNA], where η and η_0 indicate the viscosity of DNA solutions in the presence and absence of complex, respectively. The relative viscosity was calculated according to the relation $\eta = (t - t_0)/t_0$, where t is the flow time of DNA solution in the presence or absence of complex and t_0 is the flow time of the buffer alone [35]. Flow time was measured with a digital stopwatch. Each sample was measured three times and an average flow time was calculated.

The DNA cleavage experiments were carried out by agarose gel electrophoresis following a literature method [36, 37]. pUC19 DNA (0.1 μg μL^{-1}) in Tris buffer (pH = 7.2, 50 mM Tris–HCl, 18 mM NaCl) was treated with varying concentration of **1** and a fixed concentration of H_2O_2 (360 μM). The samples were incubated at 37 °C for 3 h and loading buffer was added after incubation. Then, the samples were electrophoresed for 30 min at

90 V on 1% agarose gel in Tris-Boric acid-EDTA buffer. After electrophoresis, bands were visualized by UV light and photographed by the Gel Imaging and Documentation Digi Doc-It System. Cleavage mechanistic investigation of pUC19 DNA was carried out in the presence of standard radical scavengers and reaction inhibitors. These reactions were carried out by adding standard radical scavengers of DMSO, NaN_3, SOD, EDTA, KI, and L-histidine to pBR322 DNA prior to addition of complex. The cleavage experiment was initiated by the addition of complex and quenched with 2 μL of loading buffer. Further analysis was carried out by previously described standard method.

2.5. *Cell culture*

Human cervical carcinoma cell line HeLa obtained from the American Type Culture Collection (Rockville, MD, USA) was grown in high glucose DMEM, which was supplemented with 10% FBS, 100 units/mL penicillin and 100 μg/mL streptomycin. Cells were maintained in a humidified atmosphere containing 95% air and 5% CO_2 at 37 °C.

2.6. *Cytotoxicity evaluation*

2.6.1. MTT assay. Cell viability was examined by MTT assay, which is a colorimetric assay based on the conversion of the yellow tetrazolium salt MTT to purple formazan crystals by metabolically active cells [38]. HeLa cells (1×10^4 per well) plated in 96-well plates were incubated at 37 °C in a 5% CO_2 humidified atmosphere for 24 h. Six replica wells were used for controls. Then, graded amounts of **1** at different concentrations ranging from 0 to 40 μM and cisplatin from 0 to 67 μM in 20 μL of FBS-free culture medium were added to the wells and the plates were incubated in a 5% CO_2 humidified atmosphere for 48 h. 0.1 mg of MTT (in 20 μL of phosphate buffered saline (PBS)) was added to each well, and cells were incubated at 37 °C for 4 h. Then, the supernatant was removed, and 100 μL of DMSO (stop agent) was added to dissolve the MTT formazan precipitate. The absorbance of samples was measured at 570 nm using an enzyme-linked immunosorbent assay reader. The sensitivity of HeLa to complex treatment was expressed in terms of IC_{50} (drug concentration producing 50% inhibition of cell growth, calculated on the regression line in which absorbance values at 570 nm were plotted against the logarithm of drug concentration).

2.6.2. Clonogenic survival assay. Clonogenic survival was defined as the ability of the cells to maintain their clonogenic capacity and to form colonies [39, 40]. About 500 cells per well were seeded into a six-well culture plate to form clones and varying amounts of **1** (0–40 μM) were each added to the plates on the third day in a 5% CO_2 humidified atmosphere at 37 °C. Two weeks later, cells were washed with PBS and fixed with methanol/acetic acid (3 : 1) solution for 15 min, then stained with crystal violet solution (1% crystal violet, 20% ethanol) for 30 min and rinsed with water to remove extra dye; the colonies (containing a minimum of 50 cells) were counted. The numbers of colonies in treated groups were expressed as a percentage of those in the control group.

2.7. *Apoptosis evaluation*

The morphology of HeLa cell lines after treatment was analyzed with the aid of Hoechst 33342 staining. First, 5×10^4 HeLa cell lines were seeded, respectively, into a 6-well plate

in 2 mL of medium for 24 h. Then, varying amounts of **1** were each added to the plates, which were incubated for 24 h. After washing with PBS twice, the cells were stained with Hoechst 33342 (10 μg mL^{-1}) for 15 min at 37 °C in the dark. After a final wash in PBS, samples were visualized with the aid of EPI fluorescence microscopy [41].

3. Results and discussion

3.1. *Description of crystal structure*

As shown in figure 1, **1** comprises one mononuclear Cu(II) unit and three lattice waters. Two carboxylic groups at the 2 and 6 positions in H_3ptc lose protons to balance the +2 charges of the metal ion and leave the free carboxylic acid group at the 4 position uncoordinated, which result in the $Hptc^{2-}$ anion. In the mononuclear unit, Cu(II) is six-coordinate by two carboxylic oxygens (O4, O6) and one nitrogen (N1) from tridentate chelate $Hptc^{2-}$, two nitrogens (N2, N3) from chelate Me_2bpy and one oxygen (O7) from water, forming a distorted CuN_3O_3 octahedral geometry. The *trans* bond angles N3–Cu1–N1, O7–Cu1–N2 and O6–Cu1–O4 are 176.79(10), 170.03(13) and 150.57(9), respectively. The Cu–N bond distances vary in the range of 1.972(3)–2.018(3) Å and the Cu–O bond distances are 1.988 (3) and 2.323(2) Å, which are close to literature values [42].

Extensive hydrogen bonds are formed between the oxygen atom (O7) of the coordinated water molecule in one mononuclear Cu(II) unit and the uncoordinated carboxylic oxygen atom (O3) in the adjacent mononuclear unit to form 1-D chains (figure 2(a)). The pyridyl rings of Me_2bpy in neighboring chains are parallel to each other, and there are face-to-face π–π stacking interactions between the parallel pyridyl rings, with an interplanar distance of 3.53 Å. Through the weak bonds, the 2-D plane is formed from 1-D chains (figure 2(b)). In addition, the lattice water molecules form intricate hydrogen bonds with carboxylic oxygen atoms in mononuclear units, resulting in an overall 3-D) structure (figure S1). Corresponding hydrogen bond distances and angles are listed in table S1.

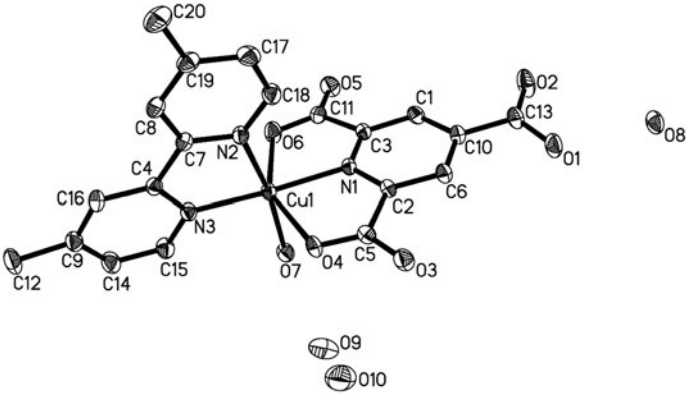

Figure 1. ORTEP diagram of $[Cu(Hptc)(Me_2bpy)(H_2O)]\cdot 3H_2O$ (**1**) showing the crystallographic numbering scheme; all hydrogens are omitted for clarity.

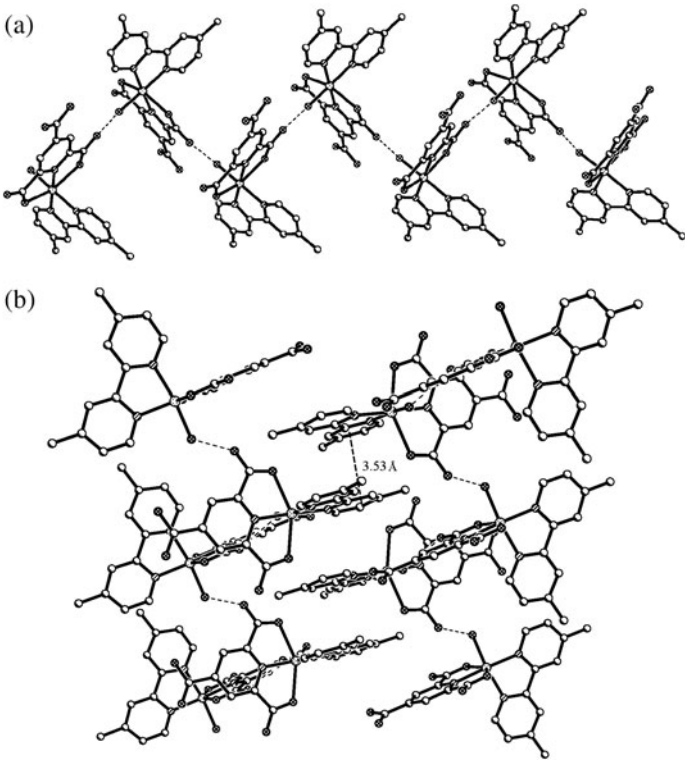

Figure 2. Views of the molecular packing diagram showing the 1-D structure with intermolecular hydrogen bonds (a) and the 2-D structure with further π–π stacking (b) between mononuclear Cu(II) units (solvate omitted for clarity).

3.2. *DNA Binding and cleavage activities*

3.2.1. UV–vis absorption spectroscopy studies. UV–vis absorption spectroscopy is one of the most common ways to investigate the interactions of complexes with DNA. The absorption spectra of **1** in the absence and presence of CT-DNA at different concentrations are given in figure 3. The absorption peaks for **1** at 208 nm and 307 nm are due to intraligand π–π* transition. With the addition of increasing amounts of CT-DNA, hypochromism of 47.8% and redshift of 7 nm are observed at the peak maximum. This suggests intercalation between the complex and DNA, because intercalation would lead to hypochromism and bathochromism in UV absorption spectrum due to the intercalative mode involving a strong stacking interaction between the aromatic chromophore of the complex and the base pairs of DNA. The extent of the hypochromism is commonly consistent with the strength of intercalative interaction [43]. The binding constant K_b was determined using the following equation [44]:

$$[\mathrm{DNA}]/(\varepsilon_a - \varepsilon_f) = [\mathrm{DNA}]/(\varepsilon_b - \varepsilon_f) + 1/K_b(\varepsilon_b - \varepsilon_f) \quad (1)$$

where [DNA] is the concentration of DNA, ε_a, ε_f, and ε_b correspond to the extinction coefficient of the complex at a given DNA concentration, the extinction coefficient of the free

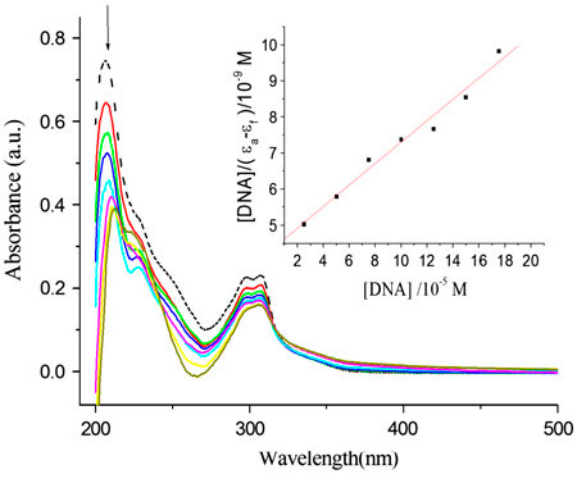

Figure 3. Absorption spectrum of complex ([complex] = 2×10^{-5} M) in the absence (dashed line) and presence (solid line) of increasing amounts of CT-DNA at room temperature in Tris–HCl/NaCl buffer (pH = 7.2). Inset: Plot of [DNA]/($\varepsilon_a - \varepsilon_f$) *vs.* [DNA] for absorption spectral titration of the complex.

complex in solution, and the extinction coefficient of the complex when fully bound to DNA, respectively. From the observed spectrophotometric changes, the value of the intrinsic binding constant K_b (6.87×10^3 M^{-1} for **1**) was determined by regression analysis using equation (1). The K_b value is lower than those reported for typical classical intercalators (e.g. EB, ~10^6 M^{-1}) [45] and those of the affinities of intercalators containing similar planar ligands [46]. Our results are consistent with some earlier reports on binding of Cu complexes to DNA [47, 48], which have similar mononuclear structures; while much lower than those of dinuclear copper(II) complexes [49] or mononuclear copper(II) complexes with benzimidazole derivative ligands [50], which possess better binding affinity due to the extended aromaticity and coplanarity for better stacking between the base pairs of DNA. The lower K_b value observed for the present complex implies that **1** does not intercalate very strongly or deeply between the DNA base pairs. We propose that the lower red shifts observed in the UV–vis spectrum are due to the partial intercalation of the pyridyl ring, because the two methyl substitutes of Me_2bpy ligand and the carboxylic acid groups of $Hptc^{2-}$ ligand in **1** may cause hindrance when the complex molecule interacts with CT-DNA. In addition, methyl, as an electron pushing group, will increase the electron density on the intercalating ligands, hence reinforcing the repulsion between the complex and DNA with the negatively charged phosphate backbone, and consequently destabilize the DNA-complex system, causing a decrease in the DNA-binding affinity [49].

3.2.2. Fluorescence spectroscopy studies. Fluorescence measurements were performed to investigate the binding ability of **1** to DNA by a MPF-4 fluorescence spectrophotometer. No luminescence could be observed for **1** at room temperature in aqueous solution, and therefore the binding of **1** to DNA is evaluated by the fluorescence emission intensity of EB bound to DNA as a probe. As one of the most sensitive fluorescence probes, EB can emit intense fluorescence at about 600 nm in the presence of DNA due to its strong intercalation between the adjacent base pairs of DNA [51], which could be quenched by the

addition of another molecule due to the decrease in the binding sites of DNA available for EB [52, 53]. The interaction of **1** with CT-DNA was studied with an EB-bound CT-DNA solution in Tris–HCl/NaCl buffer (figure 4). Fluorescence intensities at 606 nm (510 nm excitation) were measured after addition of different complex concentrations, which suggest that **1** displaces DNA-bound EB and binds to DNA at the intercalation sites with almost the same affinity. According to the Stern–Volmer equation, the relative binding propensity of the complex to CT-DNA was determined from the slope of the straight line obtained from the plot of the fluorescence intensity *versus* the complex concentration [54]. The fluorescence quenching curve of EB-bound CT-DNA by **1** showed that the quenching of EB-DNA system by **1** is in good agreement with the classical Stern–Volmer equation. From the equation $K_{EB}[EB] = K_{app}$ [complex] (where [complex] is the value at a 50% reduction of the fluorescence intensity of EB, $K_{EB} = 1.0 \times 10^7$ M^{-1}, and [EB] = 4 μM), the apparent binding constant (K_{app}) of **1** was calculated to be 5.26×10^5 M^{-1}, less than the binding constant of the classical intercalators and metallointercalators (10^7 M^{-1}, which was reported by Cory *et al.* [55]), which suggests that the interaction of **1** with DNA is a moderate intercalative mode. Such quenched fluorescence of EB bound to DNA is also found in other copper complexes and the K_{app} value is similar [56].

3.2.3. Viscosity measurements. To confirm the intercalative mode of the binding between the complex and DNA, a viscosity study was also carried out. An increase in relative viscosity reflects an increase in apparent molecular length. A molecule bound to DNA by intercalation will cause lengthening and unwinding of the DNA helix, thus leading to significant increase in viscosity of the DNA solution [57]. By contrast, groove binding and electrostatic interactions only cause slight or no changes in viscosity [58]. The viscosity experiments were carried out on CT-DNA by varying the concentration of the added complex and the corresponding data are illustrated in figure 5. Upon increasing the concentration of the complex, the specific viscosity of CT-DNA obviously increased. This result also suggests that the complex can bind to DNA in an intercalative mode [59].

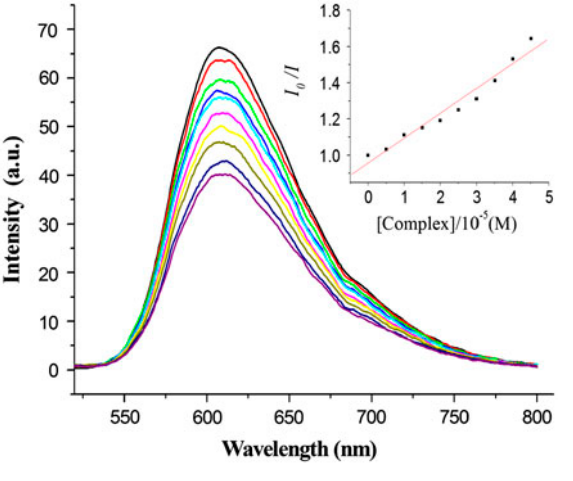

Figure 4. Fluorescence quenching curves of EB bound to DNA by **1** ([complex] = 0–4.5 × 10^{-5} M). Inset: Plot of I_0/I vs. [complex], λ_{em} = 510 nm.

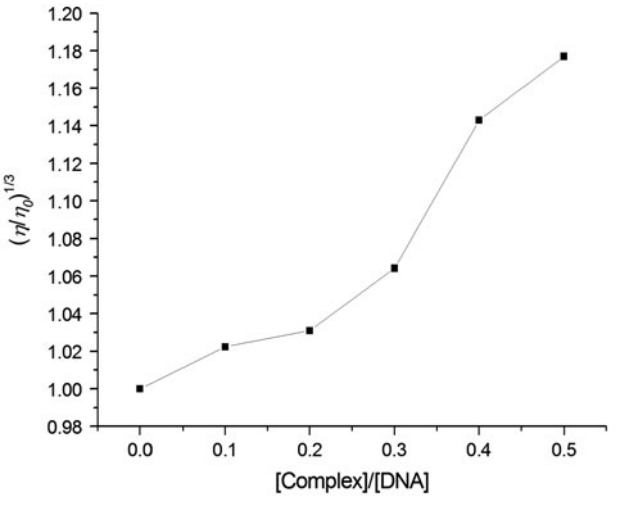

Figure 5. Effects of increasing amount of the complex on the relative viscosity of CT-DNA.

3.2.4. DNA cleavage activities. Results of gel electrophoretic separations of plasmid pUC19 DNA induced by increasing concentration of **1** in the presence of H_2O_2 is shown in figure 6. When the original supercoiled form (Form I) of plasmid DNA is nicked, an open circular relaxed form (Form II) can be found in the system. When conducted by electrophoresis, the compact Form I migrates relatively fast while the nicked Form II migrates slowly. Control experiments using only H_2O_2 did not show any significant DNA cleavage under similar experimental conditions (lane 1). With increasing concentration of **1**, Form I plasmid DNA was gradually converted into Form II. This result indicates that the copper complex can efficiently cleave plasmid DNA.

To obtain information about the active oxygen species which was responsible for the DNA damage, we investigated the DNA cleavage in the presence of H_2O_2. Depending on the number of electrons transferred from the complex to O_2, several possible intermediates, including hydroxyl radical (·OH), singlet oxygen ($^1O_2$), superoxide anion O_2^-, and hydrogen peroxide (H_2O_2), are capable of participating in the copper-mediated oxidative DNA cleavage process. To elucidate the cleavage mechanism of pUC19 plasmid DNA induced by **1**, we investigated the DNA cleavage in the presence of a hydroxyl radical scavenger

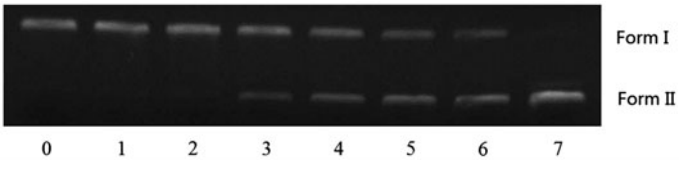

Figure 6. Gel electrophoresis showing chemical nuclease activity of **1** on pUC19 DNA (0.1 μg μL^{-1}), incubation at 37 °C for 3 h in the presence of H_2O_2. Lane 0: DNA control; lane 1: DNA + H_2O_2 (360 μM); lane 2: DNA + complex **1** (37 μM) + H_2O_2 (360 μM); lane 3: DNA + **1** (112 μM) + H_2O_2 (360 μM); lane 4: DNA + **1** (261 μM) + H_2O_2 (360 μM); lane 5: DNA + **1** (373 μM) + H_2O_2 (360 μM); lane 6: DNA + **1** (485 μM) + H_2O_2 (360 μM); lane 7: DNA + **1** (634 μM) + H_2O_2 (360 μM).

(DMSO), singlet oxygen quenchers (NaN_3, L-histidine), superoxide scavenger (SOD), hydrogen peroxide scavenger (KI) and chelating agent (EDTA) under the same conditions. As demonstrated in figure 7, no obvious inhibitions could be observed in the presence of DMSO (lane 2) and SOD (lane 4), indicating noninvolvement of hydroxyl and superoxide radicals in the cleavage reaction. The Cu^{II}-specific chelating agent, EDTA (lane 5), could efficiently inhibit DNA cleavage of **1**, suggesting that the Cu(II) complex plays a crucial role in the cleavage. Potassium iodide (lane 6) significantly diminished the nuclease activity of **1**, which is indicative of the involvement of hydrogen peroxide in the cleavage process. Addition of singlet oxygen scavengers like NaN_3 and L-histidine (lanes 3 and 7) showed apparent inhibition of nuclease, suggesting that $^1O_2$ or any other singlet oxygen-like entity may participate in the DNA strand scission [60]. The result suggests that the complex cleaves DNA through oxidative processes.

3.3. *Cytotoxicity evaluation*

3.3.1. MTT assay. The cytotoxicity of **1** against HeLa cells has been tested by MTT assay. The HeLa cells were incubated with six different concentrations of **1** and cisplatin (as a control group). Complex inhibited cell growth and induced cell death of HeLa cells in a dose-dependent manner (IC_{50} = 4.24 ± 0.03 μM), in which the IC_{50} values were calculated from the curves constructed by plotting cell survival (%) *versus* the logarithm of copper complex and cisplatin concentration (M) (figure 8). The *in vitro* cytotoxicity of **1** is considerably higher than cisplatin (IC_{50} = 15 μM) against HeLa cell lines, indicating that **1** has the potential to act as an effective metal-based anticancer drug.

3.3.2. Clonogenic assay. Colony formation assay is the gold standard for measuring the effects of cytotoxic agents on cancer cells *in vitro*, which is based on the ability of a single cell to grow into a colony. The ability of **1** to inhibit growth of HeLa cells has been evaluated by the following procedure. Cells were treated with increasing amounts of complex and the colonies that were defined to consist of at least 50 cells were counted and photographed. The number of colony-forming cells was reduced in a concentration-dependent manner by the copper complex (figure 9). The number of colony-forming HeLa cells treated with 5 μM complex was 40.2% of those of the corresponding untreated control group. No colony could be observed at the dosage of 30 μM and 40 μM. This result is consistent with

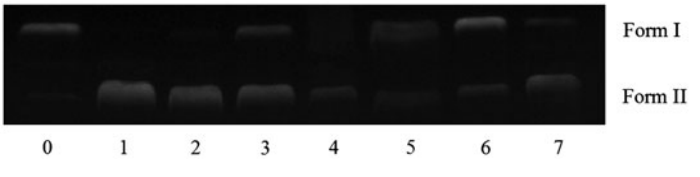

Figure 7. Agarose gel showing cleavage of pUC19 DNA (0.1 μg μL^{-1}) incubated with **1** (600 μM) in the presence of H_2O_2 (360 μM) at 37 °C for 3 h. Lane 0: DNA control; lane 1: DNA + complex + H_2O_2; lane 2: DNA + complex + H_2O_2 + DMSO (20 mM); lane 3: DNA + complex + H_2O_2 + NaN_3 (20 mM); lane 4: DNA + complex + H_2O_2 + SOD (6 units); lane 5: DNA + complex + H_2O_2 + EDTA (5 mM); lane 6: DNA + complex + H_2O_2 + KI (20 mM); lane 7: DNA + complex + H_2O_2 + L-histidine (20 mM).

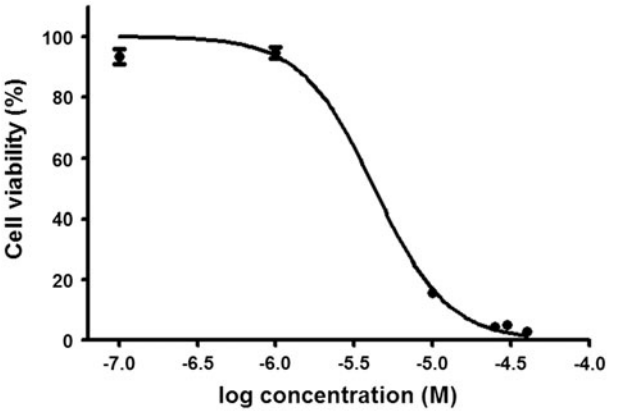

Figure 8. Dose-response curve for cell proliferation assay in HeLa cells treated with **1**. Error bars indicate ± standard deviations from the mean for six incubations.

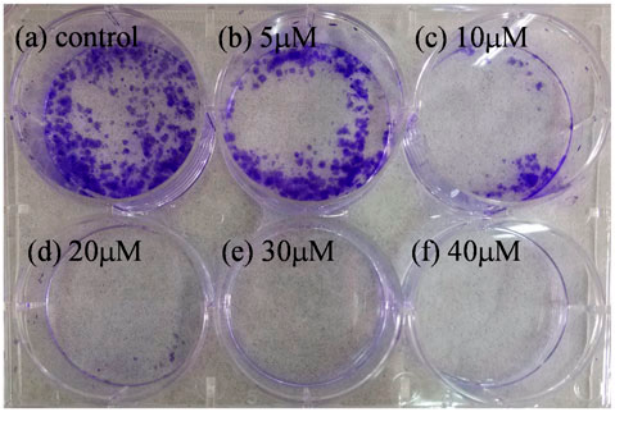

Figure 9. Clonogenic assay (crystal violet staining) in HeLa cells exposed to varying concentraiton of **1** for 48 h.

the result of the MTT assay, indicating that **1** can effectively suppress HeLa cell line growth and proliferation.

3.4. *Apoptosis evaluation by Hoechst 33342 staining*

In order to examine the nuclear morphological changes and apoptotic body formation that are characteristic of apoptosis, which is different from necrosis that refers to uncontrolled cell death, HeLa cells treated with **1** at different concentration were stained with Hoechst 33342 and visualized by fluorescent microscopy (figure 10). The bisbenzimidazole dye Hoechst 33342 is known to penetrate the plasma membrane and stain DNA in cells without permeabilization, and a stronger blue fluorescence can be observed in apoptotic cells compared with non-apoptotic cells [61]. The untreated cells with intact cell membranes showed very poor uptake of the nuclear stain after a wash with PBS (figure 10(a)), while after the HeLa cells were treated with **1** (5 μM), a small number of bright spots appeared in the nucleus (figure 10(b)), and with the concentration of complex increasing to 10 and 20 μM, an obvious change in cell

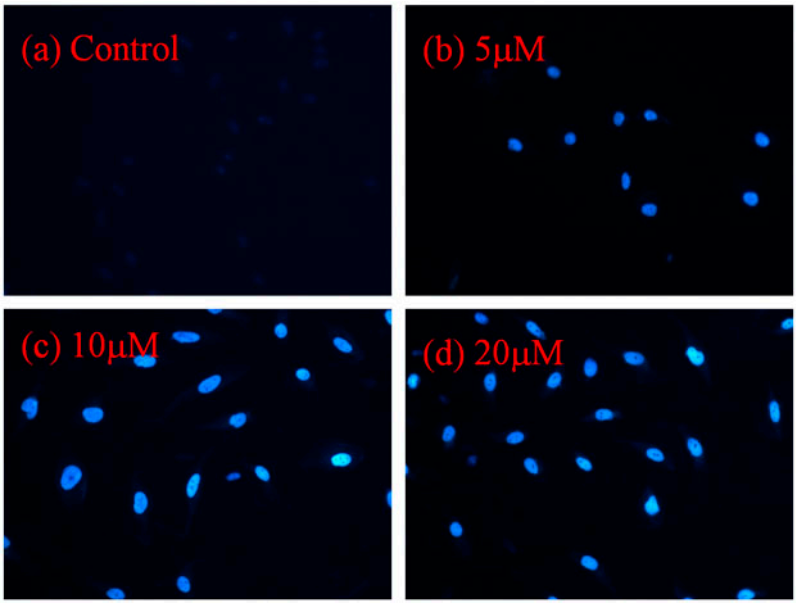

Figure 10. Apoptosis of HeLa cells induced by **1**. Morphological changes of HeLa cells treated with various concentration of **1** for 48 h which were stained with Hoechst 33258 and detected by fluorescence microscope.

morphology with apoptosis body was observed (figure 10(c) and (d)). Based on these morphologic findings, we can preliminarily conclude that **1** may induce cell death in HeLa cells through an apoptotic pathway.

4. Conclusion

A mononuclear copper(II) complex has been synthesized and characterized. Partial intercalation between the complex and CT-DNA has been confirmed by using various spectroscopic methods and viscosity. Complex **1** exhibited effective oxidative DNA cleavage activity in the presence of H_2O_2. Moreover, **1** exhibited significant cytotoxic activity toward HeLa cell lines and the IC_{50} value of **1** is considerably lower than the clinically-used cisplatin under *in vitro* conditions. The characteristics of apoptosis in cell morphology have been observed by nuclear staining with Hoechst 33342. The results from our present study suggest that **1** deserves further investigation as a new potential antitumor drug.

Supplementary material

Packing view of the 3-D structure and table of hydrogen bond distances and angles. Crystallographic data for the structure reported in this article have been deposited with the Cambridge Crystallographic Data Center, CCDC No. 934234. Copies of this information may be obtained free of charge from the Director, CCDC, 12 Union Road, Cambridge, CB2 1EZ, UK (Fax: +44-1223-336033; E-mail: deposit@ccdc.cam.ac.uk or http://www.ccdc.cam.ac.uk). Supplemental data for this article can be accessed http://dx.doi.org/10.1080/00958972.2013.857015.

Funding

This study was supported by the National Natural Science Foundation of China [grant number 21371135], [grant number 20971099]; and the Key Program of Tianjin Municipal Natural Science Foundation [grant number 13JCZDJC28200].

References

[1] M.L. Jain, P.Y. Bruice, I.E. Szabó, T.C. Bruice. *Chem. Rev.*, **112**, 1284 (2012).
[2] I. Eryazici, C.N. Moorefield, G.R. Newkome. *Chem. Rev*., **108**, 1834 (2008).
[3] V. Milacic, D. Chen, L. Ronconi, K.R. Landis-Piwowar, D. Fregona, Q.P. Dou. *Cancer Res.*, **66**, 10478 (2006).
[4] I. Kostova. *Anticancer Agents Med. Chem.*, **6**, 19 (2006).
[5] B. Rosenberg, L. Van Camp, J.E. Trosko, V.H. Mansour. *Nature*, **222**, 385 (1969).
[6] R.M. Medina, J. Rodriguez, A.G. Quiroga, F.J. Ramos-Lima, V. Moneo, A. Carnero, C. Navarro-Ranninger, M.J. Macazaga. *Chem. Biodivers.*, **5**, 2090 (2008).
[7] R. Song, K.M. Kim, Y.S. Sohn. *Inorg. Chim. Acta*, **292**, 238 (1999).
[8] M. Buczkowska, A. Bodtke, U. Lindequist, M. Gdaniec, P.J. Bednarski. *Arch. Pharm. Chem. Life Sci.*, **344**, 605 (2011).
[9] E.R. Jamieson, S.J. Lippard. *Chem. Rev.*, **99**, 2467 (1999).
[10] T.C. Kuo. *Int. J. Toxicol.*, **27**, 257 (2008).
[11] I. Tomohiro, I. Yuko, O. Kenji, O. Masayoshi, I. Munekazu, O. Yoshinori, N. Yoshinori, A. Yukihiro. *Bioorg. Med. Chem.*, **16**, 721 (2008).
[12] P.U. Maheswari, M. Ster, S. Smulders, S. Barends, G.P. Wezel, C. Massera, S. Roy, H. Dulk, P. Gamez, J. Reedijk. *Inorg. Chem.*, **47**, 3719 (2008).
[13] E.L. Hegg, J.N. Burstyn. *Coord. Chem. Rev.*, **173**, 133 (1998).
[14] Y. Jin, J.A. Cowan. *J. Am. Chem. Soc.*, **127**, 8408 (2005).
[15] F. Mancin, P. Scrimin, P. Tecilla, U. Tonellato. *Chem. Commun.*, **20**, 2540 (2005).
[16] D.K. Kenneth, S. Itoh, S. Rokita. *Copper – Oxygen Chemistry*, Wiley, UK (2010).
[17] D.R. Green, J.C. Reed. *Science*, **281**, 1309 (1998).
[18] Z.Y. Ma, X. Qiao, C.Z. Xie, J. Shao, J.Y. Xu, Z.Y. Qiang, J.S. Lou. *J. Inorg. Biochem.*, **117**, 1 (2012).
[19] J. Easmon, G. Pürstinger, G. Heinisch, T. Roth, H.H. Fiebig, W. Holzer, W. Jager, M. Jenny, J. Hofmann. *J. Med. Chem.*, **44**, 2164 (2001).
[20] F.P. Dwyer, E. Mayhew, E.M. Roe, A. Shulman. *Brit. J. Cancer*, **19**, 195 (1965).
[21] Y. Ma, L. Cao, T. Kavabata, T. Yoshino, B.B. Yang, S. Okada. *Free Radical Biol. Med.*, **25**, 568 (1998).
[22] F. Liang, C.T. Wu, H.K. Lin, T. Li, D.Z. Gao, Z.Y. Li, J. Wei, C.Y. Zheng, M.X. Sun. *Bioorg. Med. Chem. Lett.*, **13**, 2469 (2003).
[23] X. Qiao, Z.Y. Ma, C.Z. Xie, F. Xue, Y.W. Zhang, J.Y. Xu, Z.Y. Qiang, J.S. Lou, G.J. Chen, S.P. Yan. *J. Inorg. Biochem.*, **105**, 728 (2011).
[24] R. Buchtík, Z. Trávníček, J. Vančo, R. Herchel, Z. Dvořák. *Dalton Trans.*, **40**, 9404 (2011).
[25] S.H. Cui, M. Jiang, Y.T. Li, Z.Y. Wu, X.W. Li. *J. Coord. Chem.*, **64**, 4209 (2011).
[26] A. DeVizcaya-Ruiz, A. Rivero-Muller, L. Ruiz-Ramirez, G.E.N. Kass, L.R. Kelland, R.M. Orr, M. Dobrota. *Toxicol. in vitro*, **14**, 1 (2000).
[27] C. Mejia, L. Ruiz-Azuara. *Pathol. Oncol. Res.*, **14**, 467 (2008).
[28] M.E. Bravo-Gomez, J.C. Garcia-Ramos, I. Garcia-Mora, L. Ruiz-Azuara. *J. Inorg. Biochem.*, **103**, 299 (2009).
[29] L. Syper, K. Kloc, J. Mlochowski. *Tetrahedron*, **36**, 123 (1980).
[30] C.Y. Gao, X.F. Ma, J.L. Tian, D.D. Li, S.P. Yan. *J. Coord. Chem.*, **63**, 115 (2010).
[31] M.E. Reichmann, S.A. Rice, C.A. Thomas, P. Doty. *J. Am. Chem. Soc.*, **76**, 3074 (1954).
[32] Siemens. *SMART and SAINT, Area Detector Control and Integration Software*, Siemens Analytical X-ray Instruments Inc., Madison, Wisconsin, USA (1995).
[33] G.M. Sheldrick. *SADABS: Program for Empirical Absorption Correction of Area Detector Data*, University of Göttingen, Germany (1996).
[34] G.M. Sheldrick. *SHELXL-97, Program for X-ray Crystal Structure Solution*, Göttingen University, Germany (1997).
[35] S. Thalamuthu, B. Annaraj, S. Vasudevan, S. Sengupta, M.A. Meelakantan. *J. Coord. Chem.*, **66**, 1805 (2013).
[36] F. Xue, C.Z. Xie, Y.W. Zhang, Z. Qiao, X. Qiao, J.Y. Xu, S.P. Yan. *J. Inorg. Biochem.*, **115**, 78 (2012).
[37] W.H. Armstrong, S.J. Lippard. *J. Am. Chem. Soc.*, **106**, 4632 (1984).

[38] A. Ghadersohi, D. Pan, Z. Fayazi, D.G. Hicks, J.S. Winston, F.Z. Li. *Breast Cancer Res. Treat.*, **102**, 19 (2007).
[39] K.W. Yip, E. Ito, X. Mao, P.Y. Billie Au. D.W. Hedley. J.D. Mocanu. C. Bastianutto. A. Schimmer. F.-F. Liu. *Mol. Cancer Ther.*, **5**, 2234 (2006).
[40] T. Frgala, O. Kalous, R.T. Proffitt, C.P. Reynolds. *Mol. Cancer Ther.*, **6**, 886 (2007).
[41] Y.J. Lee, E. Shacter. *J. Biol. Chem.*, **274**, 19792 (1999).
[42] C.Z. Xie, R.F. Li, L.Y. Wang, Q.Q. Zhang, Z. Anorg. *Allg. Chem.*, **636**, 657 (2010).
[43] S.A. Tysoe, R.J. Morgan, A.D. Baker, T.C. Strekas. *J. Phys. Chem.*, **97**, 1707 (1993).
[44] A.M. Pyle, J.P. Rehmann, R. Meshoyrer, C.V. Kumar, N.J. Turro, J.K. Barton. *J. Am. Chem. Soc.*, **111**, 3051 (1989).
[45] J.B. Lepecq, C. Paoletti. *J. Mol. Biol.*, **27**, 87 (1967).
[46] P.R. Reddy, A. Shilpa, N. Raju, P. Raghavaiah. *J. Inorg. Biochem.*, **105**, 1603 (2011).
[47] K. Pothiraj, T. Baskaran, J. Lu, N. Raman. *J. Coord. Chem.*, **65**, 2110 (2012).
[48] C.Y. Gao, X.F. Ma, J. Lu, Z.G. Wang, J.L. Tian, S.P. Yan. *J. Coord. Chem.*, **64**, 2157 (2011).
[49] X.L. Wang, M. Jiang, Y.T. Li, Z.Y. Wu, C.W. Yan. *J. Coord. Chem.*, **66**, 1985 (2013).
[50] H.L. Wu, X.C. Huang, B. Liu, F. Kou, F. Jia, J.K. Yuan, Y. Bai. *J. Coord. Chem.*, **64**, 4383 (2011).
[51] F.J. Meyer-Almes, D. Porschke. *Biochemistry*, **32**, 4246 (1993).
[52] B.C. Baguley. M. LeBret, *Biochemistry*, **23**, 937 (1984).
[53] J. Qian, L.P. Wang, J.L. Tian, C.Z. Xie, S.P. Yan. *J. Coord. Chem.*, **65**, 122 (2012).
[54] J.R. Lakowicz, G. Webber. *Biochemistry*, **12**, 4161 (1973).
[55] M. Cory, D.D. McKee, J. Kagan, D.W. Henry, J.A. Miller. *J. Am. Chem. Soc.*, **107**, 2528 (1985).
[56] V.A. Joseph, K.M. Vyas, J.H. Pandya, V.K. Gupta, R.N. Jadeja. *J. Coord. Chem.*, **66**, 1094 (2013).
[57] Z.B. Ou, Y.H. Lu, Y.M. Liu, S. Chen, Y.H. Xiong, X.H. Zhou, Z.W. Mao, X.L. Le. *J. Coord. Chem.*, **66**, 2152 (2013).
[58] C. Icsel, V.T. Yilmaz, A. Golcu, E. Ulukaya, O. Buyukgungor. *Bioorg. Med. Chem. Lett.*, **23**, 2117 (2013).
[59] L.H. Zhi, W.N. Wu, Y. Wang, G. Sun. *J. Coord. Chem.*, **66**, 227 (2013).
[60] N. Raman, K. Pothiraj, T. Baskaran. *J. Coord. Chem.*, **64**, 4286 (2011).
[61] G. Chandrasekher, D. Sailaja. *Invest. Ophthalmol. Vis. Sci.*, **45**, 3577 (2004).